

Modification in surface properties of poly-allyl-diglycol-carbonate (CR-39) implanted by Au⁺ ions at different fluences

RIFFAT SAGHEER^{1,*}, M. SHAHID RAFIQUE², FARHAT SALEEMI¹, SHAFaq ARIF¹, FABIAN NAAB³, OVIDIU TOADER³, ARSHAD MAHMOOD⁴, RASHAD RASHID⁴, IRSHAD HUSSAIN⁵

¹Physics Department, Lahore College for Women University, Lahore, 54000, Pakistan

²Physics Department, University of Engineering and Technology, Lahore, 54000, Pakistan

³Michigan Ion Beam Laboratory, University of Michigan, Ann Arbor, MI, 48109-2104, USA

⁴National Institute of Lasers and Optronics (NILOP), P.O. Nilore, Islamabad, Pakistan

⁵Chemistry Department, Lahore University of Management Sciences, Lahore, Pakistan

Ion implantation has a potential to modify the surface properties and to produce thin conductive layers in insulating polymers. For this purpose, poly-allyl-diglycol-carbonate (CR-39) was implanted by 400 keV Au⁺ ions with ion fluences ranging from 5×10^{13} ions/cm² to 5×10^{15} ions/cm². The chemical, morphological and optical properties of implanted CR-39 were analyzed using Raman, Fourier transform infrared (FT-IR) spectroscopy, atomic force microscopy (AFM) and UV-Vis spectroscopy. The electrical conductivity of implanted samples was determined through four-point probe technique. Raman spectroscopy revealed the formation of carbonaceous structures in the implanted layer of CR-39. From FT-IR spectroscopy analysis, changes in functional groups of CR-39 after ion implantation were observed. AFM studies revealed that morphology and surface roughness of implanted samples depend on the fluence of Au ions. The optical band gap of implanted samples decreased from 3.15 eV (for pristine) to 1.05 eV (for sample implanted at 5×10^{15} ions/cm²). The electrical conductivity was observed to increase with the ion fluence. It is suggested that due to an increase in ion fluence, the carbonaceous structures formed in the implanted region are responsible for the increase in electrical conductivity.

Keywords: CR-39; ion implantation; chemical modification; optical band gap; electrical conductivity

© Wrocław University of Technology.

1. Introduction

Polymers are the type of materials having unique properties such as light weight, flexibility, high resistance to corrosion, high optical transparency, ease of processing, etc. which make them versatile in everyday life. In spite of these characteristics, their utilization in opto-electronics and electrical devices is still limited due to their high electrical resistivity [1]. There is a growing need to tailor the surface properties of polymers keeping the bulk properties unchanged [2]. Ion implantation is an effective technique through which the desired properties of polymers can be achieved in

a controlled way. Ion implantation parameters, e.g. ion type, ion energy, ion fluence, nature of polymeric material, play vital role in modifying the properties of polymers [3–6].

When an energetic ion beam is incident on the polymer, the energy is transferred to the polymer through two main processes: nuclear energy loss (ion-atom interaction) and electronic energy loss (ion-electron energy loss). As a result of these processes, different phenomena take place in the polymer, such as bond breaking, chain scissoring, cross linking, liberation of volatile molecules and defects formation. These phenomena lead to the modification in structural, chemical, optical, mechanical and electrical properties of polymer [3, 7, 8].

*E-mail: riffatlc@yahoo.com

The surface properties of many insulating polymers like polyetheretherketone (PEEK) [9, 10], polyethylene terephthalate (PET) [11, 12], polyimide (PI) [9, 10], polycarbonate (PC) [13], etc., have been tuned by ion implantation in a very controlled way. Among these polymers, poly-allyl-diglycol-carbonate (CR-39) is a transparent and colorless polymer. Its chemical formula is (C₁₂H₁₈O₇)_n. Its weight is about half the weight of glass. It has the refractive index nearly equal to that of glass. Due to these properties, CR-39 is used in making sunglasses and eye-glasses [14]. Being highly sensitive to radiations, it is widely used in the detection of radiations and ions [6].

Research is being carried out to investigate the optical properties of CR-39 after ion implantation at different implantation parameters [15–17]. However, to the best of our knowledge, the effect of ion implantation on electrical properties of CR-39 has not been investigated yet. Although very few reports are available to modify its electrical properties by neutrons [18], alpha and gamma radiations [19], yet no attempt has been performed to improve the electrical conductivity of CR-39 by ion implantation.

The objective of present research work was to modify, for the first time, the electrical properties of ion implanted CR-39, in conjunction with its chemical and optical properties. For this purpose, the polymer was implanted by Au⁺ ions with different ion fluences in the range from 5×10^{13} ions/cm² to 5×10^{15} ions/cm². The structural and chemical alterations in CR-39 induced by ion implantation were analyzed by Raman and Fourier transform infrared (FT-IR) spectroscopy. The changes produced in the optical properties of implanted CR-39 were estimated using UV-Vis spectroscopy. The effect of varying fluence of metal ions on the electrical conductivity of implanted samples was explored. The examination of surface morphology of Au⁺ ion implanted CR-39 was carried out by atomic force microscopy. The mechanism of modification in the chemical, optical, electrical and morphological properties of Au⁺ ion implanted CR-39 was discussed.

From the application perspective, the above mentioned ion fluences have been chosen so that the electrical conductivity of CR-39 after Au⁺ ion implantation was enhanced to semi-insulating range. This was an initial attempt to improve the electrical conductivity of ion implanted CR-39. In future, CR-39 with improved electrical conductivity may find applications in the field of semi-insulating devices due to the fabrication of thin conductive layer over the insulating substrate. In addition, CR-39 can be utilized in various optoelectronic devices by realizing the induced electrical conduction in the implanted layer with its induced optical behavior.

2. Experimental

2.1. Ion implantation

Transparent, flat sheet of poly-allyl-diglycol-carbonate, CR-39, with thickness of 2.75 mm was cut into rectangular pieces with dimension 2.3 cm × 1 cm. These samples were ultrasonically cleaned with deionized water. The ion implantation of polymer samples was performed under vacuum $\sim 1.33 \times 10^{-6}$ Pa at room temperature by using 400 keV Au⁺ ions with ion fluences 5×10^{13} ions/cm², 1×10^{14} ions/cm², 5×10^{14} ions/cm², 1×10^{15} ions/cm², and 5×10^{15} ions/cm² using 400 kV NEC ion implanter. The total beam current on the target was set at 0.85 μ A so that the desired ion fluence could be achieved and thermal degradation of the samples could be avoided.

2.2. Characterization techniques

The pristine and ion implanted samples were characterized by Raman, Fourier transform infrared (FT-IR) spectroscopy, atomic force microscopy, UV-Visible (UV-Vis) spectroscopy and four-point probe technique in order to explore the modifications in structural and chemical properties, surface morphology, optical and electrical properties after ion implantation. Raman spectra were recorded in the range of 400 cm⁻¹ to 3300 cm⁻¹ by Ramboss Raman spectrometer with argon laser operating at 514 nm. The FT-IR studies were carried

out in transmission mode in the range of 500 cm^{-1} to 4000 cm^{-1} using ALPHA FT-IR spectrometer with an attenuated total reflectance (ATR) assembly. Surface morphology of CR-39 after implantation was analyzed by JSPM-5200, JEOL atomic force microscope in tapping mode. The optical properties of Au^+ ion implanted CR-39 were investigated in the range of 300 nm to 900 nm using Hitachi UV-Vis U-2800 spectrometer. The DC conductivity of implanted samples was measured using four-point probe apparatus with Keithley 6220 current-source and Keithley 2182 nanovoltmeter.

2.3. SRIM/TRIM simulations

In order to proceed systematically and to avoid material wastage, it is preferable that before ion implantation, parameters of the material and the process are simulated by using the codes like SRIM/TRIM codes.

The value of electronic energy losses (S_e), nuclear energy losses (S_n) and projected range of 400 keV Au^+ ions in CR-39 samples were calculated using SRIM 2008 software [20] and are tabulated in Table 1.

Table 1. Calculated values of S_e , S_n and projected range of 400 keV Au^+ ions for CR-39.

Ion type	Energy [keV]	S_e [eV/nm]	S_n [eV/nm]	Range [nm]
Au^+	400	6.673×10^2	1.689×10^3	220

When 400 keV Au^+ ions are incident on CR-39, they transfer their energy to the polymer. As CR-39 with chemical formula $(\text{C}_{12}\text{H}_{18}\text{O}_7)_n$, has carbon, hydrogen and oxygen atoms in its structure, the energy of incident ions is absorbed by these atoms. As a result, they are knocked out from their lattice sites, leaving vacancies there. When the displaced atoms collide with other target atoms along their trajectories, they cause collision cascade in the material which dominates the damage process [21]. TRIM simulation has been performed to analyze the damages produced in CR-39 after Au^+ ion implantation [20]. Fig. 1a presents the estimated ion trajectories for 1000 Au^+ ions. It is to be mentioned here that different colors

have been used to show the tracks of the moving C, H and O atoms in the material, as labeled in Fig. 1a. The vacancies-depth distribution for 400 keV Au^+ ion implanted CR-39, estimated using TRIM simulation, is presented in Fig. 1b. The incident ions have a mean projected range of 220 nm, as given in Table 1. This is the most probable projected range of 400 keV Au^+ ions in CR-39. According to the TRIM simulations, the maximum of hydrogen vacancy distribution is at a depth of 167 nm. Much smaller number of vacancies per incident Au^+ ion is created by displacements of heavier atoms: carbon and oxygen, as shown in Fig. 1b. Due to the damage process that occurred in Au^+ ion implanted CR-39, the chemical structure of the polymer has changed.

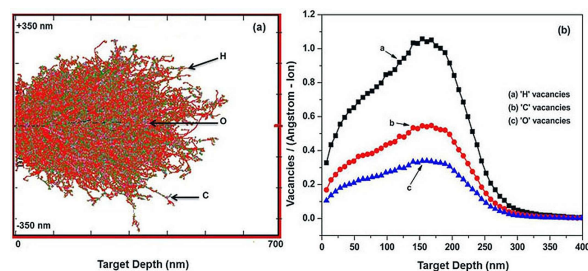


Fig. 1. SRIM/TRIM simulation for 400 keV Au^+ ion implantation in CR-39 (a) estimated ion trajectories (b) vacancies-depth distribution.

3. Results and discussion

3.1. Appearance of Au^+ implanted CR-39

The visual examination of implanted samples revealed that the color of the samples was changed after ion implantation. It was observed that the pristine CR-39 sample was transparent and colorless. The sample implanted at fluence 5×10^{13} ions/cm² appeared to have creamy color. For the sample implanted at ion fluence 1×10^{14} ions/cm², the color became pale yellow. Then the color transformed to yellowish brown, light brown and dark brown for samples implanted with ion fluences 5×10^{14} ions/cm², 1×10^{15} ions/cm², 5×10^{15} ions/cm², respectively. This color change is related to the structural modifications produced in the ion implanted polymer [22].

3.2. Raman spectroscopy

In order to analyze the chemical modifications produced in CR-39 after Au⁺ ion implantation, the Raman spectroscopy has been performed.

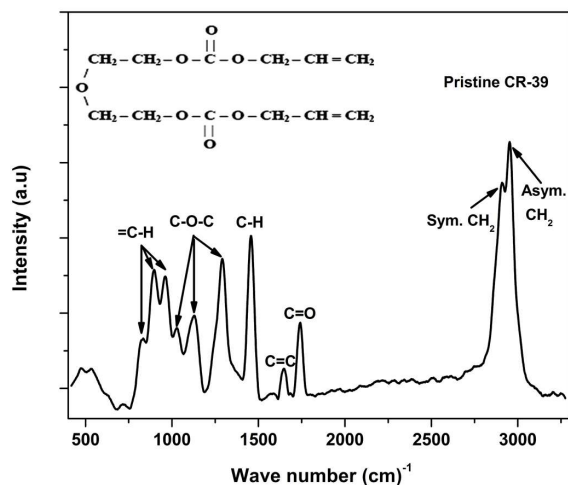


Fig. 2. Raman spectrum for pristine CR-39.

In the Raman spectrum of pristine sample (Fig. 2), several peaks occur at 828 cm⁻¹, 894 cm⁻¹, 960 cm⁻¹, 1026 cm⁻¹, 1129 cm⁻¹, 1292 cm⁻¹, 1453 cm⁻¹, 1646 cm⁻¹, 1742 cm⁻¹, 2908 cm⁻¹, 2952 cm⁻¹. The bands at 828 cm⁻¹, 894 cm⁻¹, 960 cm⁻¹ are originated from =C-H bending mode. The bands at 1026 cm⁻¹, 1129 cm⁻¹, 1292 cm⁻¹ are due to C-O-C stretching vibrations. At 1453 cm⁻¹, the medium intensity band is correlated to -C-H- bending mode. The bands at 1646 cm⁻¹, 1742 cm⁻¹ indicate the presence of C=C and C=O bonds, respectively. The highest intensity bands at 2908 cm⁻¹, 2952 cm⁻¹ are attributed to symmetric and asymmetric CH₂ stretching, respectively. From the presence of these bands, the monomer structure of CR-39 is confirmed [23].

As a result of Au⁺ ion implantation, all the bands are eliminated (Fig. 3) which points towards the polymer chain scissoring. The disappearance of bands at 2908 cm⁻¹, 2952 cm⁻¹ after implantation indicates the reduction of hydrogen content in the surface of implanted samples [24]. Such dehydrogenation may result in the formation of unsaturated

bonds and sp² carbon clusterization in implanted CR-39.

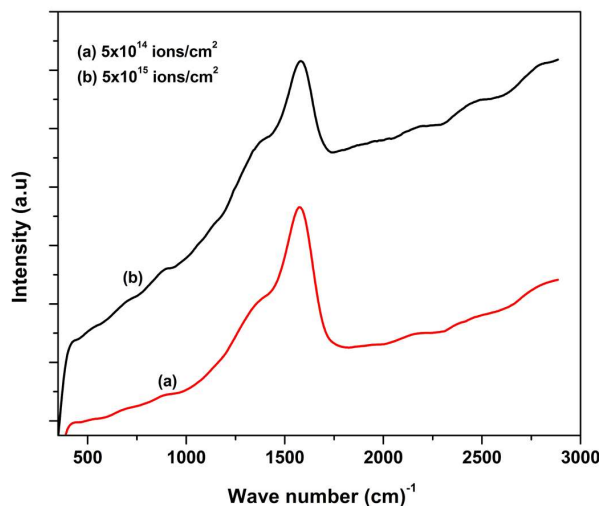


Fig. 3. Raman spectra of 400 keV Au⁺ ion implanted CR-39 at (a) 5×10^{14} ions/cm² and (b) 5×10^{15} ions/cm².

As a result of implantation (Fig. 3, curve a), the appearance of a broad band at 1577 cm⁻¹, with a big shoulder at 1391 cm⁻¹, is noticed. These two bands are named as the well-known graphite-like G and disorder D bands of hydrogenated amorphous carbon structure. The G band is correlated to the bond stretching of all pairs of sp²-atoms in both rings and chains, whereas the D band refers to the breathing mode of sp²-atoms in rings only [1]. The value of intensity ratio I_D/I_G for the ion fluence of 5×10^{14} ions/cm² was found to be 0.52. This indicates that the carbonaceous structure with small amount of sp² C-C bonding is formed in ion implanted CR-39 [1].

With further increase in ion fluence to 5×10^{15} ions/cm² (Fig. 3, curve b), the peak positions of G and D bands shift to 1582 cm⁻¹ and 1402 cm⁻¹, respectively. The ratio I_D/I_G is found to decrease to the value of 0.46. This behavior suggests that sp³ bonds are formed at high implantation fluence. This results in the ordered structure of implanted layer of CR-39 at high fluences [25].

3.3. Fourier transform infrared spectroscopy (FT-IR) studies

In order to study the changes produced in the functional groups of implanted polymer samples, FT-IR spectroscopy analysis has been carried out, as shown in Fig. 4.

In the spectrum of pristine CR-39, three strong intensity bands appear at 788 cm^{-1} , 1234 cm^{-1} and 1745 cm^{-1} corresponding to $=\text{C}-\text{H}$ bending modes [26], $\text{C}-\text{O}-\text{C}$ stretching [27] and $\text{C}=\text{O}$ stretching, respectively [26, 27]. Other weak intensity bands at 1394 cm^{-1} , 1458 cm^{-1} relate to $\text{C}-\text{H}$ bending modes, whereas the bands in the region of 1000 cm^{-1} to 1200 cm^{-1} are attributed to $\text{C}-\text{O}$ stretching mode [26]. The band at 2935 cm^{-1} is due to $\text{C}-\text{H}$ stretching [28]. The appearance of these bands at their particular wave number confirms the monomer structure of CR-39.

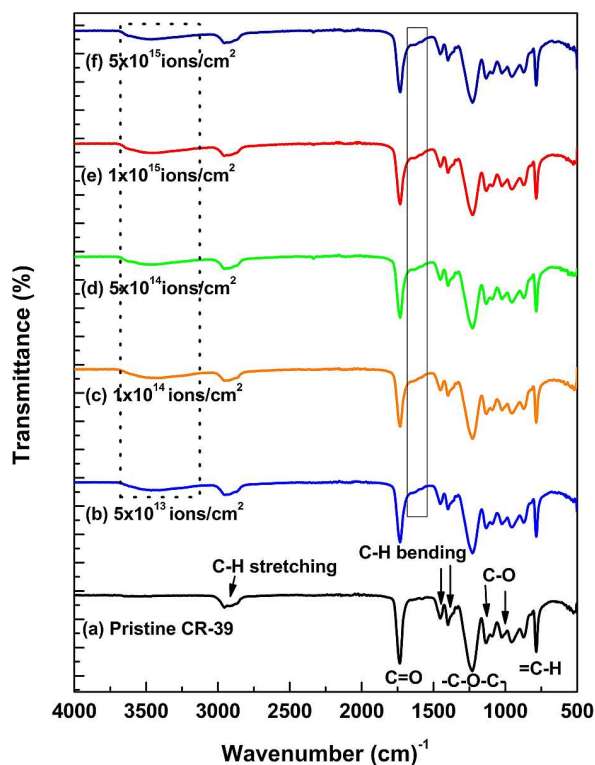


Fig. 4. FT-IR spectra of (a) pristine and implanted CR-39 with 400 keV Au^+ ion beam at (b) 5×10^{13} ions/ cm^2 (c) 1×10^{14} ions/ cm^2 (d) 5×10^{14} ions/ cm^2 (e) 1×10^{15} ions/ cm^2 (f) 5×10^{15} ions/ cm^2 .

In the spectra of CR-39 implanted by Au^+ ions with different ion fluences, the intensity of all bands of implanted samples is noticed to decrease at all ion fluences, suggesting degradation of polymer samples [28]. However, no change in the position of the bands is observed. Moreover, no prominent changes in terms of new peaks emergence are observed in the FT-IR spectra which may be due to lower sensitivity of FT-IR measurements for very thin implanted subsurface layer as only a subsurface layer with the thickness of 220 nm (SRIM estimation) is modified during implantation in comparison with the sample thickness (2.75 mm).

In addition to the overall decrease in intensity, a new broad peak appears at 3450 cm^{-1} at all ion fluences. This band corresponds to the formation of alcohol or phenol group. This suggests that free radicals are formed after chain scission at carbonate site as a result of ion implantation. These radicals react with oxygen present in air, producing OH groups. Even though the implantation was carried out in vacuum, oxidized compounds are supposed to be formed when the samples are put in air after implantation [29]. Simultaneously, a change in percentage transmittance is observed in the region of 1550 cm^{-1} to 1650 cm^{-1} which is caused by the formation of carbon-rich structures [30]. This is in agreement with the results of Raman analysis.

Thus, Raman and FT-IR spectra reveal that Au^+ ion implantation of CR-39 results in bond breaking, chain scissoring, formation of conjugated bonds and carbonaceous clusters due to which the structure of Au^+ ion implanted CR-39 is altered.

3.4. Surface morphology

In order to examine the change in surface morphology and to measure roughness values of CR-39 implanted by 400 keV Au^+ ions of different fluences, atomic force microscopy study was performed. Fig. 5 shows topographic scans of pristine and Au^+ ion implanted samples with fluences ranging from 5×10^{13} ions/ cm^2 to 5×10^{15} ions/ cm^2 .

In Fig. 5a, a relatively rough surface of pristine CR-39 is observed. Upon implantation by Au^+ ions at 5×10^{13} ions/ cm^2 , a significant change

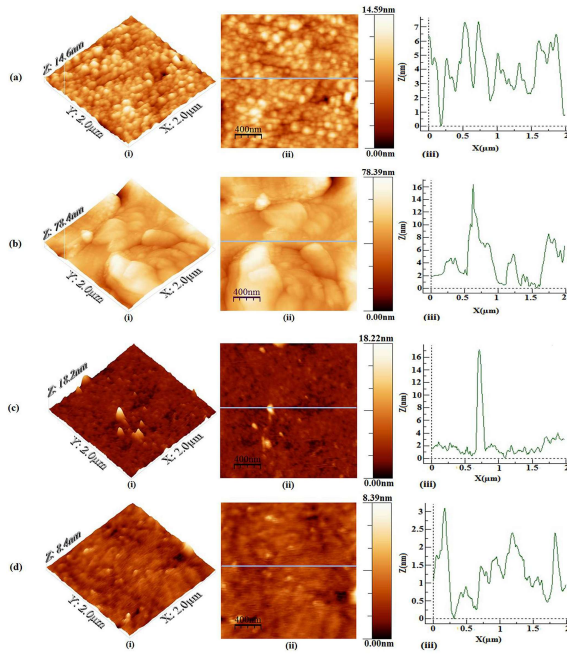


Fig. 5. Surface topography AFM images ($2 \mu\text{m} \times 2 \mu\text{m}$) of (a) pristine CR-39 and implanted by 400 keV Au⁺ ions at (b) 5×10^{13} ions/cm² (c) 5×10^{14} ions/cm² (d) 5×10^{15} ions/cm². The images on the left hand side of the figure are three-dimensional AFM micrographs, two-dimensional topographic scans are in the middle, while line profiles of surface, highlighted in the 2D images, are shown on the right hand side of the figure.

in the surface topography is obtained. Compared to the virgin sample, the one implanted by Au at 5×10^{13} ions/cm² shows the appearance of newly formed grain-like features and consequently increase in surface roughness. The surface swelling of the implanted sample is also noticed, as is presented in Fig. 5b. During implantation, Au⁺ ions are being neutralized along their way in the sample. As a result, Au atoms are produced which occupy a near surface region up to the target depth [31]. Since the kinetic energy of implanted Au⁺ ions is rather high along the longitudinal direction of implanted sample, it contributes to local temperature increase in addition to the diffusion of Au atoms. It causes the surface swelling of the implanted sample [32]. Increasing the implantation

fluence to 5×10^{14} ions/cm², spiky cone phases with average diameter of 100 nm to 200 nm and height of 5 nm to 12 nm, become visible on the implanted sample as shown in Fig. 5c. According to thermal spike model, when the temperature of cylindrical volume in the ion track reaches the melt phase, the material pushes out from the surface and is quenched by thermal conduction [33]. For the highest implantation fluence, the spikes are slightly revealed but their surface density is increased as observed in Fig. 5d.

The root mean square roughness (RMS) of pristine and Au⁺ ion implanted CR-39 at different fluences is given in Table 2.

Table 2. RMS roughness of pristine and 400 keV Au⁺ ion implanted CR-39 samples at different ion fluences.

Fluence [ions/cm ²]	RMS roughness [nm]
Pristine	1.71
5×10^{13}	8.95
5×10^{14}	1.02
5×10^{15}	0.66

It is clear from the Table 2 that RMS roughness of 8.95 nm is achieved already for the lowest implantation fluence. At ion fluence of 5×10^{14} ions/cm², the roughness value decreased to 1.02 nm and finally at the ion fluence of 5×10^{15} ions/cm², the root mean square roughness was reduced to 0.66 nm. These observations are in good agreement with the Raman analysis described earlier, where at highest implantation fluence, the implanted layer of CR-39 is more diamond-like carbon than that implanted at 1×10^{15} ions/cm². Upon interaction of Au ions with the polymer at high fluences, the large chains in the structure are broken and side chains are formed which easily pack and recombine. As a result, the implanted surface becomes smoother, leading to the decrease in surface roughness [32]. Such a two-stage behavior was also observed in case of high density polyethylene implanted by Ag⁺ ions at different fluences [31].

Due to the changes observed in the structure and surface morphology of CR-39 after ion

implantation, its optical and electrical properties in the implanted layer are modified.

3.5. UV-Vis spectroscopy

3.5.1. Absorption spectroscopy

Fig. 6 presents optical absorption spectra of pristine and Au⁺ ion implanted CR-39 polymer with various ion fluences (5×10^{13} ions/cm², 1×10^{14} ions/cm², 5×10^{14} ions/cm², 1×10^{15} ions/cm², 5×10^{15} ions/cm²).

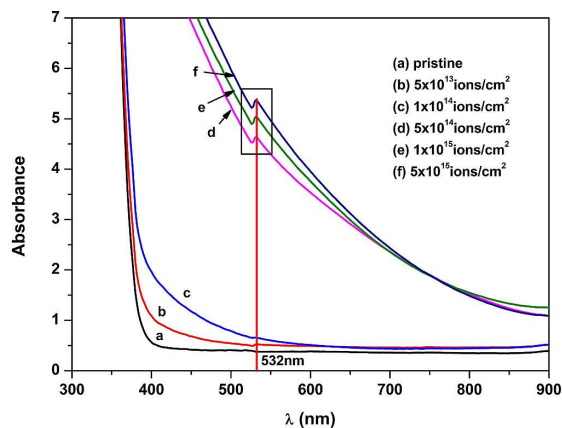


Fig. 6. UV-Vis absorption spectra of CR-39 (a) pristine and implanted at 400 keV to (b) 5×10^{13} Au⁺ ions/cm², (c) 1×10^{14} Au⁺ ions/cm², (d) 5×10^{14} Au⁺ ions/cm², (e) 1×10^{15} Au⁺ ions/cm², (f) 5×10^{15} Au⁺ ions/cm².

It is observed that absorption of pristine sample falls to the base level at 420 nm with a sharp absorption edge. For the ion implanted samples, there is a shift of absorption edge towards longer wavelengths with the increase in ion fluence. When the energetic ions are incident on the polymer surface, several processes, such as bond breaking, chain scissoring, cross linking, formation of free radicals, formation of defects and new bonds occur in the polymer simultaneously, as discussed earlier in Raman and FT-IR studies. As a result of these processes, the absorption edge of the ion implanted samples shifts towards longer wavelengths [1, 32, 34]. It is clear from Fig. 6 that the sharpness of band edge of implanted samples is decreased with the increase in ion fluence and tends to be flattened.

This broadening of the band edge is attributed to the increase in optical density due to the formation of carbon-rich structures [35, 36], evidenced through Raman and FT-IR analysis. The absorption spectra of implanted samples are almost the same at ion fluences of 5×10^{14} ions/cm², 1×10^{15} ions/cm², and 5×10^{14} ions/cm². A shoulder like peak exists at 532 nm for these ion fluences as mentioned in Fig. 6. This peak is associated to the deformation of valence band or/and the formation of defect bands in the forbidden band as a result of ion implantation [36].

3.5.2. Energy band gap

The optical band gap energy of the polymer can be calculated from the optical absorption spectra using the Tauc's relation [37]:

$$\alpha(h\nu) = B(h\nu - E_g)^n/h\nu \quad (1)$$

where α is absorption coefficient, B is a constant known as transition probability, $h\nu$ is the energy of photons, E_g is the band gap energy, n is a numerical constant determining the electronic transition to be direct or indirect [38]. As CR-39 is an amorphous polymer, the indirect band gap energy was calculated by putting $n = 2$ in equation 1. By drawing a graph between $(\alpha h\nu)^{1/2}$ and $h\nu$ and extrapolating the linear portion of the graph to the energy axis, the optical band gap energy of pristine and Au implanted CR-39 has been calculated (Fig. 7) and are presented in Table 3.

It has been observed from Table 3 that optical band gap is decreased from 3.15 eV (for pristine CR-39) to 1.05 eV (for Au⁺ ion implanted CR-39 at fluence 5×10^{15} ions/cm²). This decrease in optical band gap is correlated to the formation of unsaturated bonds [36]. These unsaturated bonds contain carbon-enriched clusters in which $\pi-\pi^*$ transitions of delocalized electrons take place. Less amount of energy is required for these transitions to take place, thereby reducing the band gap energy [26, 38]. Thus, the reduction in optical band gap energy is in agreement with the observed structural changes in CR-39 after Au implantation.

Table 3. Variation of optical band gap energy E_g [eV], % decrease in band gap energy and Urbach energy E_u [eV], with different implanted fluences of CR-39.

Fluence [ions/cm ²]	Optical band gap energy E_g [eV]	% decrease in band gap energy	Urbach energy E_u [eV]
Pristine	3.15	–	0.17
5×10^{13}	3.06	2.86	0.35
1×10^{14}	2.94	6.67	0.68
5×10^{14}	1.14	64	0.88
1×10^{15}	1.10	65	0.90
5×10^{15}	1.05	67	0.91

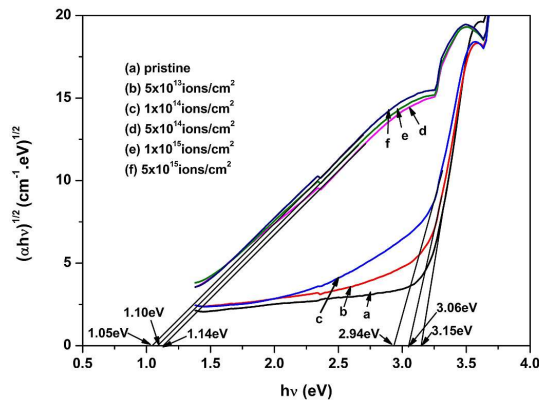


Fig. 7. Plots of $(\alpha hv)^{1/2}$ vs. (hv) to determine optical band gap energy of CR-39 polymer (a) pristine and implanted at 400 keV to (b) 5×10^{13} Au⁺ ions/cm², (c) 1×10^{14} Au⁺ ions/cm², (d) 5×10^{14} Au⁺ ions/cm², (e) 1×10^{15} Au⁺ ions/cm², (f) 5×10^{15} Au⁺ ions/cm².

The optical band gap energy and % decrease in band gap energy as functions of ion fluence, are graphically represented in Fig. 8.

During implantation the number of carbon atoms per cluster increases with the increase in ion fluence [1, 25]. When the incident ion beam transfers its energy to the host material, C–H bonds are broken and hydrogen molecules are ejected. As a result, unsaturated bonds, containing carbon-enriched domains, are formed [39].

The absorption coefficient α can be calculated from the absorbance A using the relation [36]:

$$\alpha = \frac{2.303A}{l} \quad (2)$$

where l is the thickness of the sample in cm.

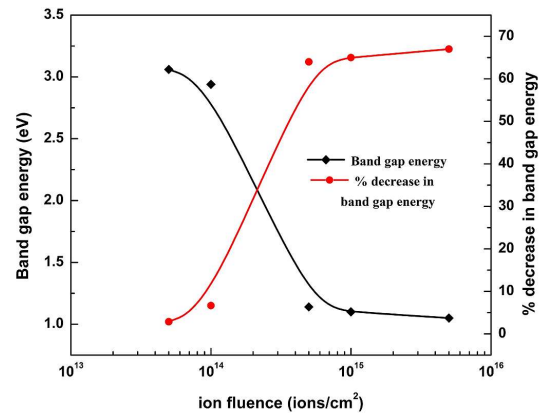


Fig. 8. Plot of optical band gap energy (E_g) and % decrease in band gap energy vs. ion fluence.

3.5.3. Urbach energy

For non-crystalline materials, the absorption coefficient α , near the band edge, depends on the photon energy $h\nu$ exponentially according to the Urbach relation [36]:

$$\alpha(h\nu) = \alpha_0 \exp(h\nu/E_u) \quad (3)$$

where α_0 is a constant. E_u is called Urbach energy. It measures the content of disordered structures produced in the polymeric materials as a result of ion implantation [22]. The value of Urbach energy (E_u) is calculated from the plots of $(\ln \alpha)$ as a function of photon energy ($h\nu$) as shown in Fig. 9.

In Fig. 9, the reciprocal of the slopes of the linear part of the curves in the lower photon energy region give the values of E_u and are tabulated in Table 3. It is observed that the Urbach energy is increased from 0.17 eV (for pristine CR-39)

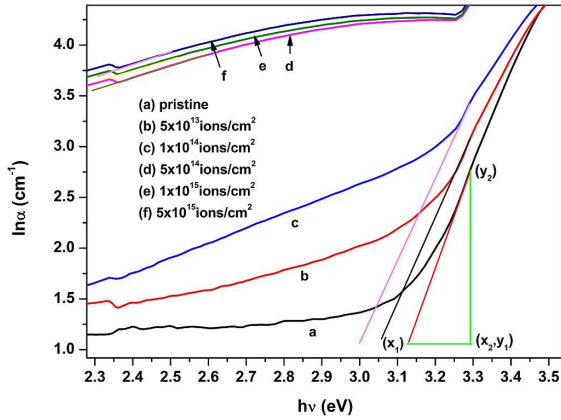


Fig. 9. Plots of $\ln(\alpha)$ vs. $(h\nu)$ to determine Urbach energy of CR-39 (a) pristine and implanted at 400 keV to (b) 5×10^{13} Au^+ ions/ cm^2 , (c) 1×10^{14} Au^+ ions/ cm^2 , (d) 5×10^{14} Au^+ ions/ cm^2 , (e) 1×10^{15} Au^+ ions/ cm^2 , (f) 5×10^{15} Au^+ ions/ cm^2 .

to 0.91 eV (for Au^+ ion implanted CR-39 at the fluence of 5×10^{15} ions/ cm^2). This indicates the widening of band tail with increasing ion fluences, leading to the enhancement of local density of the states of structural disorder [40].

The dependence of Urbach energy on the ion fluence has been established and the results are graphically represented in Fig. 10.

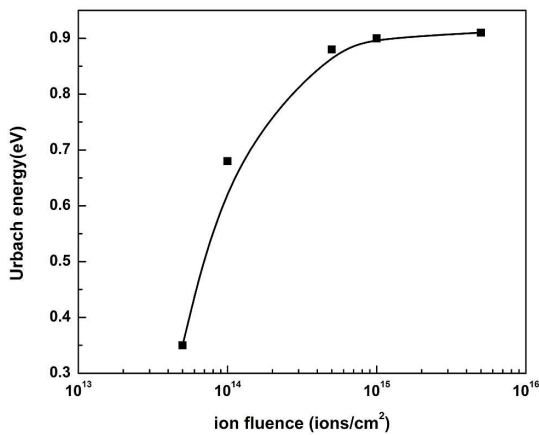


Fig. 10. Urbach energy vs. ion fluence for 400 keV Au^+ ion implanted CR-39.

From Fig. 10, it can be inferred that the Urbach energy of the implanted CR-39 is increased with

the ion fluence due to high concentration of disordered carbon content [6]. These carbonaceous clusters are supposed to be the main absorbing centers in the specimen. Thus, the absorption of implanted samples is increased while the transmission is decreased [22]. As a result, the change in color of the samples, from transparent (pristine) to dark brown at highest ion fluence (5×10^{15} ions/ cm^2), is observed.

3.6. Electrical properties

In order to investigate the modification produced in the electrical properties of metal ion implanted CR-39, the DC electrical conductivity was measured for pristine and Au^+ ion implanted CR-39. The obtained results are, thus, presented in Table 4.

Table 4. Electrical conductivity of pristine and 400 keV Au^+ ion implanted CR-39 with different ion fluences.

Fluence [ions/ cm^2]	Electrical conductivity [[$\Omega \cdot \text{cm}$] $^{-1}$]
Pristine	6.84×10^{-09}
5×10^{13}	7.41×10^{-07}
1×10^{14}	7.45×10^{-07}
5×10^{14}	7.64×10^{-07}
1×10^{15}	1.06×10^{-06}
5×10^{15}	6.52×10^{-06}

It is observed that the electrical conductivity of implanted samples is enhanced significantly in comparison with that of pristine sample. With the increase in ion fluence, the electrical conductivity of implanted samples goes on increasing and approaches a value of $6.52 \times 10^{-06} (\Omega \cdot \text{cm})^{-1}$ at maximum ion fluence of 5×10^{15} ions/ cm^2 . Since the electrical conductivity of semi-insulating materials lies in the range of $10^{-6} (\Omega \cdot \text{cm})^{-1}$ to $10^{-9} (\Omega \cdot \text{cm})^{-1}$, it can be inferred that Au^+ ion implanted CR-39 can be utilized in different semi-insulating devices.

The reason for the observed increase in electrical conductivity of implanted samples with respect to that of pristine sample is the formation of extended system of conjugated

bonds in the implanted samples [1], as already has been confirmed from Raman studies. The delocalized π -electrons are formed in the carbonaceous clusters as a result of sp^3 - sp^2 rehybridization [41]. Thus, carbon clusters act as charge carriers/conductive paths in the implanted samples. With the increase in ion fluence, the growth of carbon clusters is increased. Thus, charge carrier density is increased. In these conductive islands, the delocalized π -electrons move through hopping between the islands. This hopping current enhances the electrical conductivity of implanted samples [1].

A correlation has been established between the optical and electrical properties of implanted samples with the increase in ion fluence. The carbon-enriched domains are formed due to disordering produced in the implanted CR-39 as a result of ion implantation. The optical band gap of implanted CR-39 is decreased, while electrical conductivity of the polymer is increased after ion implantation. On the basis of these results, it can be inferred that ion implanted CR-39 can be utilized in various opto-electronic devices.

4. Conclusions

The modification in chemical structure and formation of carbonaceous clusters in the implanted layer of CR-39 were evidenced through Raman and FT-IR spectroscopy. The amorphous nature of CR-39 implanted by 400 keV Au⁺ ions was decreased at high fluences, which was revealed by Raman analysis. AFM studies revealed that the surface roughness of implanted samples was decreased at high ion fluences. As a result of structural changes produced in implanted samples, the optical band gap of CR-39 was decreased from 3.15 eV (for pristine) to 1.05 eV (for sample implanted at 5×10^{15} ions/cm²). The disorder content in the structure of CR-39 was found to increase with the increase in ion fluence. The electrical conductivity of implanted samples was increased with the increase in ion fluence, confirming the observed decrease in optical band gap energy. This work demonstrated that the surface

properties of CR-39 can be tailored by metal ion implantation for its utilization in various semi-insulating and opto-electronic devices.

Acknowledgements

The authors express their thanks to Dr. Arshad Saleem Bhatti, the Department of Physics, COMSATS, Islamabad, for providing the facility of Raman Spectrometer.

References

- [1] GOYAL P.K., KUMAR V., GUPTA R., MAHENDIA S., ANITA, KUMAR S., *Vacuum*, 86 (2012), 1087.
- [2] HADJICHRISTOV G.B., GUEORGUIE V.K., IVANOV T.Z.E., MARINOV Y.G., IVANOV V.G., FAULQUES E., *Org. Electron.*, 9 (2008), 1051.
- [3] GIROLAMO G.D., *Sensor. Actuat. A-Phys.*, 178 (2012), 136.
- [4] MALINSKY P., MACKOVA A., HNATOWICZ V., KHAIBULLIN R.I., VALEEV V.F., SLEPICKA P., SVORCIK V., SLOUF M., PERINA V., *Nucl. Instrum. Meth. B*, 272 (2012), 396.
- [5] NENADOVIC M., POTOCNIK J., MITRIC M., STRBAC S., RAKOCEVIC Z., *Mater. Chem. Phys.*, 142 (2013), 633.
- [6] NEGI A., SEMWAL A., CHANDRA S., HARIWAL R.V., SONKAWADE R.G., KANJILAL D., RANA J.M.S., RAMOLA R.C., *Radiat. Meas.*, 46 (2011), 127.
- [7] ZAKI M.F., *Braz. J. Phys.*, 38 (2008), 558.
- [8] KULSHRESTHA V., AWASTHI K., ACHARYA N.K., SINGH M., BHAGWAT P.V., VIJAY Y.K., *Polym. Bull.*, 56 (2006), 427.
- [9] TAVENNER E., WOOD B., CURRY M., JANKOVIC A., PATEL R., *Appl. Surf. Sci.*, 283 (2013), 154.
- [10] MACKOVA A., MALINSKY P., MIKSOVA R., KHAIBULLIN R.I., VALEEV V.F., SVORCIK V., SLEPICKA P., SLOUF M., *Appl. Surf. Sci.*, 275 (2013), 311.
- [11] YUANG W., TONGHE Z., YAWEN Z., GU Z., HUIXING Z., XIAOJI Z., *Surf. Coat. Tech.*, 148 (2001), 221.
- [12] WU Y., ZHANG T., ZHANG H., ZHANG X., DENG Z., ZHOU G., *Nucl. Instrum. Meth. B*, 169 (2000), 89.
- [13] RODRIGUEZ R.J., GARCÍA J.A., SÁNCHEZ R., PÉREZ A., GARRIDO B., MORANTE J., *Surf. Coat. Tech.*, 158–159 (2002), 636.
- [14] BUTT M.Z., ALI D., NAJM-UL-AARIFEEN, NASEEM S., *Physica B*, 454 (2014), 179.
- [15] ABDUL-KADER A.M., EL-BADRY B.A., ZAKI M.F., HEGAZY T.M., HASHEM H.M., *Philos. Mag.*, 90 (2010), 2543.
- [16] VIRK H.S., SRIVASTAVA A.K., *Radiat. Meas.*, 34 (2001), 65.
- [17] SHEKHAWAT N., SHARMA A., AGGARWAL S., NAIR K.G.M., *Adv. Mater. Res.*, 665 (2013), 214.
- [18] NOUH S.A., ABDEL-SALAM M.H., MORSY A.A., *Radiat. Meas.*, 37 (2003), 25.

- [19] PHUKAN T., DWIVEDI K.K., GOSWAMI D.T., DAS H.L., *Radiat. Meas.*, 33 (2001), 841.
- [20] ZIEGLER J.F., BIRSACK J.P., *The Stopping and Range of Ions in Matter*, in: BROMLEY D.A. (Ed.), *Treatise on Heavy-Ion Science. Volume 6: Astrophysics, Chemistry, and Condensed Matter*, Springer, New York, 1985, p. 93
- [21] RODRÍGUEZ J., MEDRANO A., GARCÍA J.A., FUENTES G.G., MARTÍNEZ R., PUERTOLAS J.A., *Surf. Coat. Tech.*, 201 (2007), 8146.
- [22] SHEKHAWAT N., AGGARWAL S., SHARMA A., SHARMA S.K., DESHPANDE S.K., NAIR K.G.M., *J. Appl. Phys.*, 109 (2011), 083513.
- [23] KUMAR V., GOYAL P.K., MAHENDIA S., GUPTA R., SHARMA T., KUMAR S., *Radiat. Eff. Defect. S.*, 166 (2) (2011), 109.
- [24] CHEN J.S., LAU S.P., SUN Z., TAY B.K., YU G.Q., ZHU F.Y., ZHU D.Z., XU H.J., *Surf. Coat. Tech.*, 138 (2001), 33.
- [25] RESTA V., QUARTA G., LOMASCOLO M., MARUCIO L., CALCAGNILE L., *Vacuum*, 116 (2015), 82.
- [26] GUPTA R., KUMAR V., GOYAL P.K., KUMAR S., KALSI P.C., GOYAL S.L., *Adv. Appl. Sci. Res.*, 2 (2011), 248.
- [27] ABDUL-KADER A.M., *Radiat. Meas.*, 69 (2014), 1.
- [28] KUMAR V., SONKAWADE R.G., CHAKARVARTI S.K., KULRIYA P., KANT K., SINGH N.L., DHALI WAL A.S., *Vacuum*, 86 (2011), 275.
- [29] SINGH L., SAMRA K.S., SINGH R., *Nucl. Instrum. Meth. B*, 255 (2007), 350.
- [30] GUENTHER M., GERLACH G., SUCHANECK G., SAHRE K., EICHHORN K.J., WOLF B., DEINEKA A., JASTRABIK L., *Surf. Coat. Tech.*, 158–159 (2002), 108.
- [31] STRBAC S., NENADOVIC M., RAJAKOVIC L.J., RAKOCEVIC Z., *Appl. Surf. Sci.*, 256 (2010), 3895.
- [32] POPOK V.N., *Rev. Adv. Mater. Sci.*, 30 (2012), 1.
- [33] SUN Y., ZHU Z., WANG Z., LIU J., JIN Y., HOU M., WANG Y., DUAN J., *Nucl. Instrum. Meth. B*, 212 (2003), 211.
- [34] KUMAR V., SONKAWADE R.G., CHAKARVARTI S.K., SINGH P., DHALI WAL A.S., *Radiat. Phys. Chem.*, 81 (2012), 652.
- [35] PHUKAN T., KANJILAL D., GOSWAMI T.D., DAS H.L., *Radiat. Meas.*, 36 (2003), 611.
- [36] KUMAR R., SINGH P., *Results Phys.*, 3 (2013), 122.
- [37] ALI D., BUTT M.Z., NASEEM S., *Radiat. Eff. Defect. S.*, 168 (2013), 1.
- [38] NATHAWAT R., VIJAY Y.K., *Compos. Interface.*, 17 (2010), 229.
- [39] EL-BADRY B.A., ZAKI M.F., ABDUL-KADER A.M., HEGAZY T.M., MORSY A.A., *Vacuum*, 83 (2009), 1138.
- [40] DAS A., DHARA S., PATNAIK A., *Nucl. Instrum. Meth. B*, 149 (1999), 53.
- [41] PHILIPP P., BISCHOFF L., TRESKE U., SCHMIDT B., FIEDLER J., HUBNER R., *Carbon*, 80 (2014), 677.

Received 2015-08-30

Accepted 2016-05-20